

Chapter 3

High-Speed, Ultra-High-Precision Nanopositioning: A Signal Transformation Approach

Ali Bazaei, Yuen K. Yong, S.O. Reza Moheimani, and Abu Sebastian

Abstract. Signal transformation is a novel strategy employed in feedback control to reduce the impact of measurement noise on positioning accuracy. This chapter addresses robustness issues of the method with respect to output disturbance and uncertainty in plant low frequency gain. The robustness problems can be solved by an inner loop with integral action before incorporating the signal transformation mappings. Feedback controllers are designed for two-dimensional positioning of a novel 12-electrode piezoelectric tube used for scanning probe microscopy. The closed-loop bandwidths are intentionally limited to set the standard deviation of the projected noise around 0.1 nm. For triangular waveform tracking and a general class of plants and compensators, necessary and almost sufficient conditions are derived for stability and convergence of tracking error. Effectiveness of the proposed method, regarding tracking and robust performances, is shown by simulations and experiments.

3.1 Introduction

Observation, control, and manipulation of matter at very small dimensions have attracted a great amount of attention in nanotechnology (1; 2). The invention of scanning probe microscopy (SPM) is one of the revolutionary events in nanoscience and nanotechnology (3; 4; 5).

Ali Bazaei · Yuen K. Yong · S.O. Reza Moheimani
School of Electrical Engineering and Computer Science,
The University of Newcastle Australia, Callaghan, NSW 2308, Australia
email:{Ali.Bazaei, Yuenkuan.Yong,
Reza.Moheimani}@newcastle.edu.au

Abu Sebastian
IBM Research – Zurich,
8803 Rüschlikon, Switzerland
e-mail: ase@zurich.ibm.com

Accurate tracking of a fast triangular waveform is one of the major challenges not only in SPM (6; 7; 8) but also in other scanner-based devices such as optical scanners and selective laser sintering (SLS) machines (9; 10). The performance of the piezoelectric tube scanner is often quantified by its positioning resolution (which is governed by measurement noise), tracking bandwidth and robustness to disturbances (5). There has been a significant effort to improve the tracking accuracy and speed of piezoelectric tube scanners using feedback control techniques. To track a fast triangular signal, high bandwidth closed-loop controllers have been implemented in many nanopositioning devices (7; 11; 12). However, the scanning speed is limited in feedback control systems due to hysteresis, thermal drift, sensor noise, uncertainty, and mechanical vibrations when piezoelectric tubes are used to follow non-smooth triangular trajectories (13). Capacitive and inductive sensors are commonly used in nanopositioning systems due to their capability of providing simple solution for non-contact, high-resolution measurement. These sensors typically have a noise density of $20 \text{ pm}/\sqrt{\text{Hz}}$ (14). For every hundredfold increment in the closed-loop system bandwidth, the position accuracy of a nanopositioning scanner will decrease tenfold. This potentially degrades the resolution of the scanner, hindering it from performing positioning tasks that require subnanometer resolution. Hence, feedback control methods with limited closed-loop bandwidth are of considerable importance.

Command pre-shaping methods can be considered as a possible way for vibration suppression in an already designed closed-loop control system, leaving the closed-loop bandwidth of the measurement noise unaffected (15; 16; 17; 18). However, these methods are not suitable for tracking of time-varying commands such as triangular waveforms or suffer from lack of robustness to plant uncertainties. Iterative learning control (ILC) can also be added as a feed-forward control action in a feedback system to improve the steady-state tracking error for repetitive references without altering the closed-loop bandwidth (19; 9). However, it may require a large number of iterations to converge. Feedback control methods such as repetitive control (RC) for tracking of periodic references introduce large closed-loop bandwidths, which may not be acceptable in the presence of measurement noise. Moreover, the trade-off between the tracking error and rejection of non-periodic disturbances in RC systems can cause problems when excessive cross coupling exist among the scanner axes (20; 21).

In (22), the concept of signal transformation was put forward as a novel approach for tracking of triangular waveforms in a nanopositioning system. The method showed significant closed-loop performance improvement compared with an ordinary feedback-control-system having a similar control bandwidth. However, the method is sensitive to DC gain variations and disturbances arising from cross coupling between the two axes.

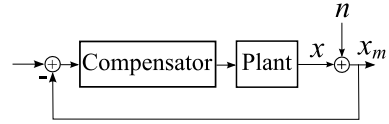
This chapter addresses how signal transformation can be used along with traditional feedback control methods to improve tracking error in an atomic force microscope (AFM) scanner while keeping closed-loop measurement noise below a pre-specified level and providing stability and robustness to DC-gain variations and

disturbances. A thorough stability analysis of the method in the absence of measurement noise and disturbances is also presented in the Appendix.

3.2 Objectives

To characterize the impact of measurement noise in feedback control systems, concept of projected noise is introduced. As shown in Fig. 3.1, consider a typical feedback control system designed to control a physical quantity x , which is measured by a sensor, that provides a measured signal $x_m := x + n$ for feedback, which is affected by measurement noise n . By the projected noise, we mean the direct effect of the measurement noise signal n on the actual controlled output x in the closed-loop feedback system. For linear systems, this effect can be quantified in terms of the noise signal n and the closed-loop transfer function from n to x . An objective in this paper is to evaluate the capability of signal transformation method in reducing projected measurement noise compared to ordinary feedback systems. To do this, we maintain the standard deviation of the projected measurement noise around 0.1nm at the actual displacement of x-axis. The other objective is to provide disturbance rejection capability and robustness when signal transformation is incorporated into the control systems.

Fig. 3.1 Illustration of projected measurement noise in a typical feedback control system



3.3 Signal Transformation

The signal transformation approach incorporates appropriate mappings between non-smooth signals (e.g. triangular waveforms) and smooth signals (e.g. ramps) in a control system to improve the tracking error while keeping the closed-loop bandwidth low to limit the projected measurement noise (22). The signal transformation method for control of a SISO plant is described by the hybrid control system shown in Fig. 3.2, where Φ and Φ^{-1} refer to the signal transformation mappings, which in the case of triangular signal tracking use piecewise constant gains g_1 and g_2 as well as biases b_1 and b_2 . The latter can be presented in the following form:

$$g_1 = g_2 = (-1)^k, \quad b_2 = 2a_0k, \quad b_1 = -(-1)^k b_2, \quad (3.1)$$

where a_0 is the amplitude of the desired triangular waveform x_d , which has period $2T$, as shown in the left top insert in Fig. 3.2, and k is the index of the half period defined as

$$k(t) = \text{floor} \left(\frac{t}{T} + 0.5 \right). \quad (3.2)$$

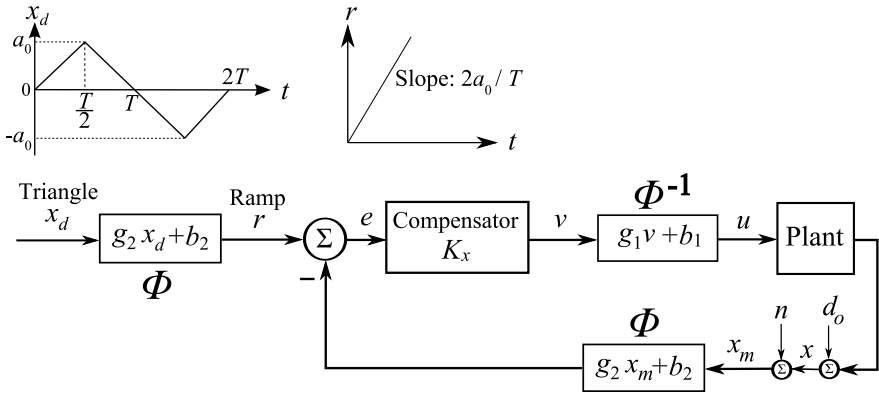


Fig. 3.2 Schematic diagram of signal transformation method for triangular waveform tracking

The signal transformation blocks, which use g_2 and b_2 , can convert the non-smooth periodic triangular signal x_d into a smooth ramp signal denoted by r in the left top insert in Fig. 3.2. The signal transformation block between the plant and compensator does the reverse action, i.e. it can convert the smooth ramp signal into the non-smooth triangular signal. Consider an ideal situation, where the noise n and output disturbance d_o are zero, the plant is a unity gain transfer function, and its output is perfectly following the desired signal. In this case, the input/output signals at the compensator block will be smooth signals with no breaks or discontinuities, and the burden of providing appropriate non-smooth trajectories at the actuator, which demands a high control bandwidth in an ordinary feedback system, is carried by the signal transformation block. In this way, the compensator can be designed with a smaller closed-loop bandwidth in favor of rejecting the projected measurement noise without deteriorating the steady-state error. The Appendix addresses necessary and sufficient stability conditions of the signal transformation method in the absence of noise and disturbances. The signal transformation method, however, has robustness and disturbance rejection problems, which will be explained in Sec. 3.4.

3.4 Investigation of System Robustness

In this section, we use simulations to show that the signal transformation method mentioned in Sec. 3.3 can improve the tracking performance of feedback control systems with low closed-loop bandwidth, which translates into low projected noise. We also investigate the robustness of the method to DC gain variations and output disturbance using a model obtained for the x-axis of an AFM scanner. To do this, we use a model for the x-axis of the scanner, obtained after closing a damping loop through a low noise piezoelectric induced voltage to damp the first resonance of the tube. The piezoelectric induced voltage is obtained as in (23). The model has zeros at $230 \pm 6000i$, $-1180 \pm 876i$, and -2.1 , and poles at $-1286 \pm 1992i$, $-1100 \pm 1497i$,

and -2.3 . A constant gain of $1/0.42$ was included at the input to force a unity DC gain for the plant in Fig. 3.2. The compensator in Fig. 3.2 is a double integrator plus an integrator in the following form:

$$K_x(s) = 2.3 \times \frac{50s + 250}{s^2}, \quad (3.3)$$

which provides a gain margin of 23.4 dB, a phase margin of 87° , and reduces the closed-loop bandwidth to 21 Hz. Such a low closed-loop bandwidth can keep the projected measurement noise around 0.1 nm, as shown in Sec. 3.6.1. For a 10-Hz triangular reference with amplitude $a_0 = 2$ V (10 μm peak-to-peak) and under different conditions, the resulting closed-loop steady-state displacement errors ($x_d - x$), scaled to voltage by sensitivity of capacitive displacement sensors (0.4 V/ μm), are shown in Fig. 3.3. With unity DC gain and no disturbance, the signal transformation provides acceptable tracking (compare the thick solid line curve with a 4-V peak-to-peak triangular reference). However, when the plant DC gain is increased or is reduced twice (6 dB), which is much less than the gain margin, the error increases unacceptably, as shown in Fig. 3.3. This shows a lack of robustness against variations in the plant DC gain. With unity plant DC gain, the steady-state error of the system to the triangular reference along with a unity amplitude constant output disturbance d_o has also been included in Fig. 3.3 (dotted line), which shows an undesirable disturbance rejection performance. In this example, the 21 Hz bandwidth with signal transformation cannot provide acceptable disturbance rejection, while it is suitable for tracking in the absence of disturbances. To appreciate the benefit of signal transformation, we have replaced the signal transformation blocks by unity gains. The resulting ordinary feedback system with unity plant DC gain and no disturbances has the response labeled “No signal transformation” in Fig. 3.3, which shows that the 21 Hz bandwidth without signal transformation is not sufficient for acceptable tracking of a 10 Hz triangular reference.

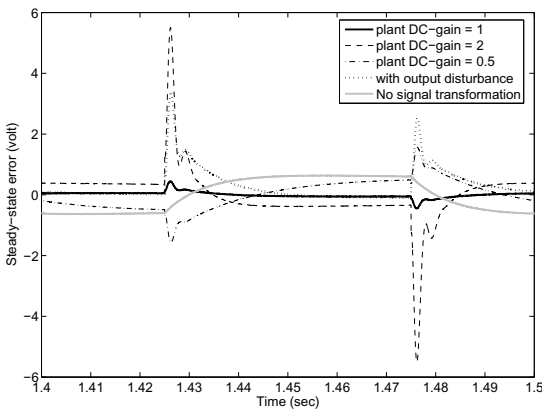


Fig. 3.3 Effects of plant DC-gain variations and output disturbance on closed-loop steady-state response of x-axis with signal transformation

3.5 Incorporating Robustness in Signal Transformation

In this section, we incorporate an intermediate feedback loop prior to the signal transformation blocks, as shown in Fig. 3.4, to improve the robustness properties mentioned in Sec. 3.4. In Fig. 3.4, the signal transformation mappings denoted by Φ and Φ^{-1} are as before, and d_{ox} , n_x , v_{cx} , v_{px} , and u_x stand for output disturbance, measurement noise, capacitive sensor output, piezoelectric induced voltage, and piezoelectric actuation voltage of the x-axis, respectively. A low-pass filter $F(s) = \left(1 + \frac{s}{1000}\right)^{-1}$ was used to reduce the effect of measurement noise. The intermediate and outer compensators were selected as

$$K_i(s) = \frac{166.667}{s} \quad (3.4)$$

$$K_{ii}(s) = \frac{50s + 250}{s^2} \quad (3.5)$$

The compensators $K_i(s)$ and $K_{ii}(s)$ were selected such that the overall transfer function from sensor noise n_x to the real displacement output signal x has a low bandwidth of 21 Hz, similar as in Sec. 3.4. This transfer function can be described as

$$T_{xn}(s) := \frac{x(s)}{n_x(s)} = -\frac{K_i(s)P_x(s)[F(s) + K_{ii}(s)]}{1 + K_i(s)P_x(s)[F(s) + K_{ii}(s)]}, \quad (3.6)$$

where $P_x(s)$ is the transfer function of the damped system of the x-axis. The robustification loop by itself (excluding the outer loop) provides a unity DC gain from u to x with a gain margin of 27.7 dB, phase margin of 90° , and bandwidth of 13 Hz. The overall system has a gain margin of 42 dB, phase margin of 55° , and bandwidth of 11.6 Hz for the forward transfer function from the reference to the displacement output. The simulation results shown in Fig. 3.5 correspond to closed-loop response of the proposed method where the same triangular reference signal and disturbance as in Sec. 3.4 are used and the plant DC gain in the legend refers to the DC gain of the damped system in Fig. 3.4. Clearly, the steady-state tracking error remains acceptable in the presence of DC-gain variations of the plant and output disturbance,

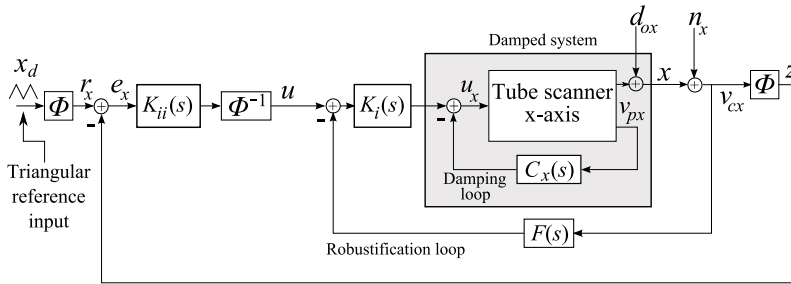


Fig. 3.4 Schematic diagram of signal transformation method with a robustification loop

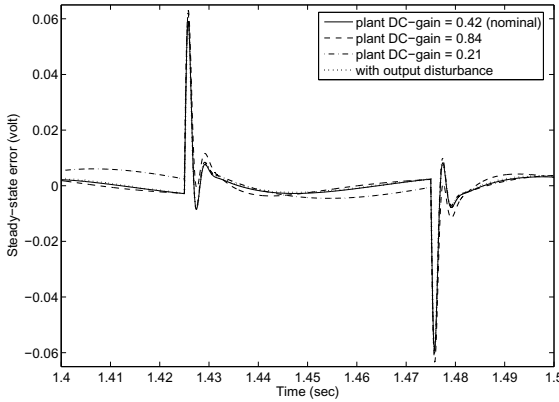


Fig. 3.5 Effects of plant DC-gain variations and output disturbance on closed-loop steady-state response of x-axis with robustified signal transformation

which shows that the robustification loop can improve the robustness of the signal transformation method without deteriorating its benefits (low tracking error with low bandwidth).

3.6 Experimental Results

In this section, the signal transformation method with the proposed robustifying scheme is performed on the x-axis of the actual scanner for further examination. The external electrode of the piezoelectric tube scanner is segmented into 12 equal sections, and the inner electrode is a continuous electrode which is grounded. One end of the tube is fixed. The free end serves as a stage over which a sample can be placed and its horizontal deflections are measured by two capacitive sensors. Figure 3.6 illustrates the wiring of the tube for actuation and sensing in the x-axis alone, where $\pm \hat{u}_x$ and \hat{v}_{px} are the actuation and piezoelectric induced voltages after and before amplification, respectively. The same wiring is applied to the y-axis, but is not illustrated for the sake of clarity. A dSPACE-1103 rapid prototyping system was

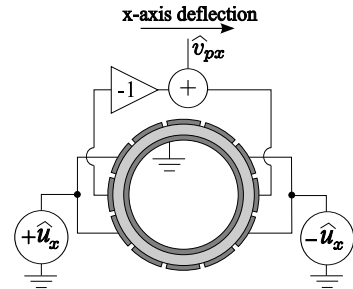
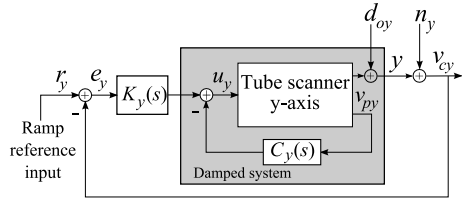


Fig. 3.6 Simultaneous piezoelectric actuation and sensing for x-axis of the tube scanner

Fig. 3.7 Schematic diagram for control of y-axis



used to implement the x- and y-axis feedback controllers in real time. The z-axis displacement was controlled using the AFM's software and circuitry. The damped y-axis is controlled by an ordinary integral control as shown in Fig. 3.7, where the compensator

$$K_y(s) = \frac{1500}{s} \quad (3.7)$$

provides a gain margin 8.2 dB and a phase margin 86° . The y-axis reference signal r_y is a ramp signal whose slope is 512 times less than that of the x-axis triangular reference. The x-axis controllers and the triangular reference signal are as in Sec. 3.5. The overall noise transfer function $T_{yn}(s)$ for the x-axis controller has a bandwidth of 21 Hz as before. A calibration grating (MikroMasch TGQ1) with a $3 \mu\text{m}$ period, $1.5 \mu\text{m}$ square side and 20 nm height was used for imaging. A contact mode ContAl cantilever probe with a resonance frequency of 13 kHz was used to perform the scan. To evaluate the scanning performance of the controllers, a 9.8 Hz triangular reference signal was applied to the x-axis and the aforementioned synchronized ramp signal was applied to the y-axis of the piezoelectric tube scanner to generate a $10 \mu\text{m} \times 10 \mu\text{m}$ image (with 256×256 scan lines). Figure 3.8(a) shows the scanned image and the tracking performance of the x-axis displacement with signal transformation of the piezoelectric tube scanner. The RMS error of the tracking signal is 80 nm.

3.6.1 Tracking Performance and Noise

The resolution of the piezoelectric tube is often governed by the sensor noise due to the noise being fed back to the actuator in closed-loop systems. This makes the open-loop architecture a more attractive solution than the closed-loop one. However, open-loop devices are sensitive to nonlinear effects such as drift and creep. These effects deteriorate the tracking performance and subsequently degrade the image quality generated by the devices.

The signal transformation method presented in this paper ensures that the noise content of the controlled x-position signal x , in Fig. 3.4, is low. To estimate the noise content of the x-axis displacement, the capacitive sensor output was first recorded as the noise signal n_x while the piezoelectric tube remained stationary. Then by simulation the response of the noise transfer function $T_{xn}(s)$ to the recorded noise signal was obtained as a measure of noise projected into the actual x-position. The

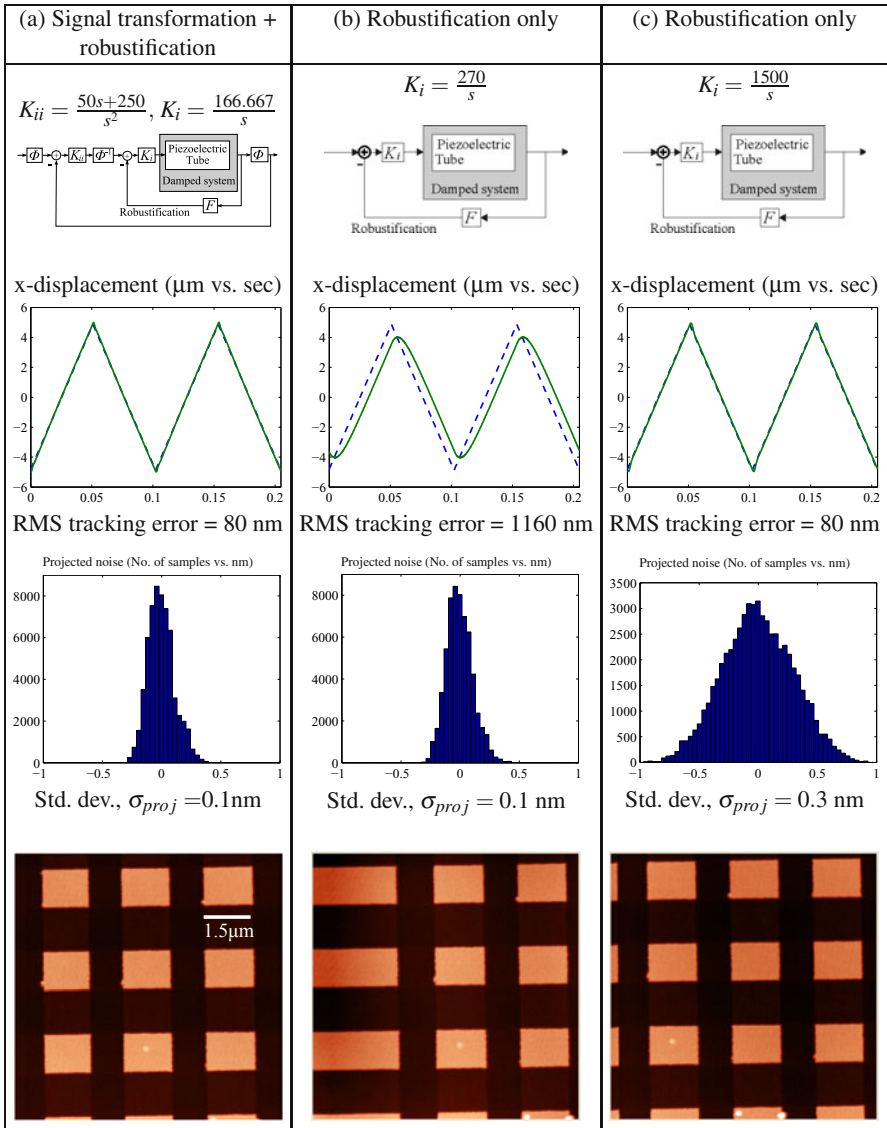


Fig. 3.8 Comparison of the projected noise, tracking error and AFM image ($10\ \mu\text{m} \times 10\ \mu\text{m}$) of the three closed-loop systems. (a) Closed-loop system with signal transformation and robustification loop. (b) Closed-loop system without signal transformation. The integrator gain was tuned to 270; therefore the projected noise is similar to that of system (a). (c) Closed-loop system without signal transformation. The integrator gain was tuned to 1500; therefore the tracking performance is similar to that of system (a). σ_{proj} is the standard deviation of the projected noise. The tracking performance in the x-axis of each closed-loop system is illustrated. The triangular reference signal (dashed line) and output displacement (solid line) are also plotted.

resulting histogram is shown in Fig. 3.8(a). The standard deviations of the sensor noise n_x and the projected noise are 3.075 nm and 0.11 nm, respectively. To evaluate the efficacy of signal transformation, we now consider an ordinary feedback system with the same level of projected noise for comparison purposes. If we remove the double integrator and the signal transformation blocks, keep the robustification and damping loops, apply the triangular reference signal at u in Fig. 3.4, and increase the integrator gain in Eq. (3.4) to 270 to have the same standard deviation of 0.11 nm for the projected noise, we obtain the resulting steady-state tracking error of the x -axis as shown in Fig. 3.8(b), where the root-mean-square (RMS) tracking error is 14.5 times more than that of the signal-transformation method. This tracking error is mostly contributed by the low closed-loop bandwidth of the system.

Alternatively, if in the latter system, which has no signal transformation, we increase the integrator gain of the x -channel to 1500 to keep the RMS value of the resulting steady-state tracking error equal to that with signal transformation, the standard deviation of the projected noise will increase to 0.3 nm, as shown in Fig. 3.8(c), which is almost three times more than that obtained with signal transformation. Thus, signal transformation with the proposed robustification loop provides better tracking performance, while keeping both the projected measurement noise and robustness against disturbance and parameter variations low.

For all three controllers designed above, the corresponding images of the calibration grating have been included in Fig. 3.8. The severe distortions in the center image are caused by the poor tracking performance of the second controller. The images of the first and the third controller are undistinguishable because of the similar tracking performance of the two controllers. The image quality of the two closed-loop systems is the same; it is determined by the sensor as well as environmental noise.

Acknowledgements. The authors wish to thank IBM Research – Zurich Research and the ARC Centre of Excellence for Complex Dynamic Systems and Control for their support of this work. Special thanks go to Evangelos Eleftheriou and Haris Pozidis for their support.

References

- [1] Devasia, S., Eleftheriou, E., Moheimani, S.O.R.: IEEE Trans. Control Systems Technol. 15(5), 802 (2007)
- [2] Sugimoto, Y., Pou, P., Custance, O., Jelinek, P., Abe, M., Pérez, R., Morita, S.: Science 322, 413 (2008)
- [3] Bhushan, B.: Nanotribology and Nanomechanics. An Introduction. Springer, Heidelberg (2005)
- [4] Kalinin, S., Gruverman, A.: Scanning Probe Microscopy: Electrical and Electromechanical Phenomena at the Nanoscale. Springer, Heidelberg (2006)
- [5] Salapaka, S., Salapaka, M.: IEEE Control Systems Mag. 28(2), 65 (2008)
- [6] Lining, S., Changhai, R., Weibin, R., Ligu, C., Minxiu, K.: J. Micromechan. Microeng. 14(11), 1439 (2004)

- [7] Mahmood, I.A., Moheimani, S.O.R., Liu, K.: *IEEE Trans. Nanotechnology* 8(1), 55 (2009)
- [8] Payam, A., Yazdanpanah, M., Fathipour, M.: In: *Proceedings 2009 4th IEEE Int'l Conf. on Nano/Micro Engineered and Molecular Systems*, pp. 717–721 (2009)
- [9] Yen, J.Y., Yeh, Y.C., Peng, Y.H., Lee, J.F.: *Mechatronics* 19(1), 65 (2009)
- [10] Zhiqiang, D., Zude, Z., Wu, A., Youping, C.: *The Int'l J. Adv. Manufacturing Technol.* 32(11-12), 1211 (2007)
- [11] Salapaka, S., Sebastian, A., Cleveland, J.P., Salapaka, M.V.: *Rev. Sci. Instrum.* 73(9), 3232 (2002)
- [12] Yong, Y.K., Aphale, S., Moheimani, S.O.R.: *IEEE Trans. Nanotechnology* 8(1), 46 (2009)
- [13] Moheimani, S.O.R.: *Rev. Sci. Instrum.* 79(7), 071101 (2008)
- [14] Fleming, A.J., Wills, A., Moheimani, S.O.R.: *IEEE Trans. Control Systems Technol.* 16(6), 1265 (2008)
- [15] Smith, O.J.M.: *Feedback Control Systems*. McGraw-Hill, New York (1958)
- [16] Singer, N.C., Seering, W.P.: *J. Dynamic Syst., Measurement, and Control* 112(1), 76 (1990)
- [17] Pennacchi, P.: *Shock and Vibration* 11(3/4), 377 (2004)
- [18] Kogiso, K., Hirata, K.: *Robotics and Autonomous Syst.* 57(3), 289 (2009)
- [19] Tien, S., Zou, Q., Devasia, S.: *IEEE Trans. Control Systems Technol.* 13(6), 921 (2005), doi:10.1109/TCST.2005.854334
- [20] Pipeleers, G., Demeulenaere, B., Al-Bender, F., De Schutter, J., Swevers, J.: *IEEE Trans. Control Systems Technol.* 17(4), 970 (2009), doi:10.1109/TCST.2009.2014358
- [21] Aridogan, U., Shan, Y., Leang, K.K.: *ASME J. Dynamic Syst., Measurement, and Control* 131(6), 061103 (2009)
- [22] Sebastian, A., Moheimani, S.O.R.: *Rev. Sci. Instrum.* 80, 076101 (2009)
- [23] Moheimani, S.O.R., Yong, Y.K.: *Rev. Sci. Instrum.* 79(7), 073702 (2008)

Appendix

Here the stability of the proposed signal transformation method in Fig. 3.2 is investigated in the absence of noise and disturbances.

Stability Analysis

We assume that the plant and compensator dynamics are of degrees n_p and n_c and are described by linear-time-invariant state-space matrix sets $[A_p, B_p, C_p]$ and $[A_c, B_c, C_c]$ with X_p and X_c referring to the corresponding state vectors, respectively. The feedthrough matrices have been assumed zero. To start the analysis, we merge the plant and its adjacent signal transformation blocks into a unified state-space model, called *equivalent plant*. Hence, we wish to determine under what circumstances the simple control system shown in Fig. 3.9 is equivalent to the original hybrid control system in Fig. 3.2, i.e., with the same ramp signal $r(t)$ in both control systems, the time histories of variables e , v , X_c , and y in the equivalent system shown in Fig. 3.9 are the same as the corresponding variables in the original system shown in Fig. 3.2.

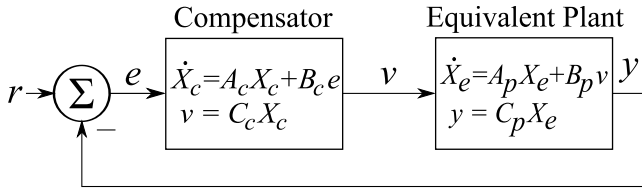


Fig. 3.9 Schematic diagram of the equivalent control system

The following theorem provides the conditions for the foregoing equivalence.

Theorem 3.1. *In a time interval $t \in (kT - \frac{T}{2}, kT + \frac{T}{2})$, the hybrid control system in Fig. 3.2 is equivalent to the control system in Fig. 3.9, and state X_e of the equivalent plant is related to the plant state by*

$$X_e := \frac{1}{g_1}(X_p + F), \quad F := A_p^{-1}B_p b_1, \quad (3.8)$$

provided that the gains and biases are constants (in the time interval) satisfying the following relationships

$$g_1 g_2 = 1, \quad b_2 - g_2 C_p A_p^{-1} B_p b_1 = 0, \quad (3.9)$$

and the equivalent state vector at the start of the time interval is initialized according to (3.8).

Proof. The signal transformations in Fig. 3.2 are described in the following forms.

$$u = g_1 v + b_1 \quad (3.10)$$

$$y = g_2 x + b_2. \quad (3.11)$$

Consider the time interval $t \in (iT - T, iT)$. Since the gain and bias signals are constant in this interval, the following state-space model is readily obtained using the plant state dynamics and Eqs. (3.10) and (3.11), if the plant has a no poles at the origin:

$$\begin{cases} \dot{X}_e = A_p X_e + B_p v \\ y = g_1 g_2 C_p X_e + (b_2 + g_2 \delta_0 b_1) \end{cases}, \quad (3.12)$$

where $\delta_0 = -C_p A_p^{-1} B_p$ is the DC gain of the plant. It is clear from Eq. (3.12) that we can replace the blocks between nodes v and y in Fig. 3.2 with the equivalent plant, as described by Fig. 3.9 and Eq. (3.8), and the control systems are equivalent if the conditions mentioned in Theorem 3.1 are satisfied.

Conditions (3.9) are satisfied with the selected gains and biases in Eqs. (3.1) if the plant has a unity DC gain ($\delta_0 = 1$). If the plant has a transfer function of the form:

$$P_{ol}(s) := \frac{x(s)}{u(s)} = \frac{\delta_0 + \delta_1 s + \cdots + \delta_{n_p-1} s^{n_p-1}}{1 + \varepsilon_1 s + \cdots + \varepsilon_{n_p} s^{n_p}}, \quad (3.13)$$

its state-space realization can be written by the following canonical form:

$$\begin{aligned} A_p &= \begin{bmatrix} 0_{(n_p-1) \times 1}, I_{n_p-1}; \frac{-1}{\varepsilon_{n_p}}, \frac{-\varepsilon_1}{\varepsilon_{n_p}}, \dots, \frac{\varepsilon_{n_p-1}}{-\varepsilon_{n_p}} \end{bmatrix}, \\ B_p &= \begin{bmatrix} 0_{(n_p-1) \times 1}; \frac{1}{\varepsilon_{n_p}} \end{bmatrix}, C_p = [\delta_0, \dots, \delta_{n_p-1}]. \end{aligned} \quad (3.14)$$

The overall state vector X of the equivalent closed-loop system, defined as

$$X := \begin{bmatrix} X_e \\ X_c \end{bmatrix}, \quad (3.15)$$

obeys the following state-space equation:

$$\begin{cases} \dot{X} = AX + Br \\ y = CX \end{cases}, \quad (3.16)$$

where

$$\begin{aligned} A &:= \begin{bmatrix} A_p & B_p C_c \\ -B_c C_p & A_c \end{bmatrix}, B := \begin{bmatrix} 0_{n_p \times 1} \\ B_c \end{bmatrix}, \\ C &:= [C_p \ 0_{1 \times n_c}]. \end{aligned} \quad (3.17)$$

The equivalent plant state X_e must be initialized by (3.8) at the start of each half period, which requires knowledge of plant state X_p . To use the equivalent control

system as a stand-alone machinery for analysis, appropriate formulas are necessary to update the equivalent state at the switching moments $t = kT - \frac{T}{2}$. The following theorem gives the updating relationships at the switching moments.

Theorem 3.2. *With the triangular reference signal shown in Fig. 3.2, signal transformation parameters (3.1), and unity DC gain for the plant, the overall state vector of the equivalent control system just before a switching moment obeys the recursive formula:*

$$X_1^- := X(T^-/2) = E^{1/2}X_0 + H + A^{-1}Ba_0, \quad (3.18)$$

$$X_{k+1}^- := X(t)|_{t=kT-\frac{T}{2}} = \hat{A}X_k^- + J(k-0.5) + H, \quad k = 1, 2, 3, \dots, \quad (3.19)$$

and the state just after a switching moment is updated using its value just before the switching moment as

$$X_k^+ := X\left(kT^+ - \frac{T}{2}\right) = \hat{I}X_k^- + L(k-0.5), \quad k = 1, 2, 3, \dots, \quad (3.20)$$

where L is the constant $(n_p + n_c) \times 1$ vector:

$$L := [4a_0, 0, \dots, 0]^T, \quad (3.21)$$

and

$$\hat{I} := \begin{bmatrix} -I_{n_p} & 0 \\ 0 & I_{n_c} \end{bmatrix}, \quad X_0 := \begin{bmatrix} X_p(0) \\ X_c(0) \end{bmatrix}, \quad (3.22)$$

$$E := e^{AT}, \quad H := 2 \left[\frac{1}{T}(E - I)A^{-1} - I \right] A^{-1}Ba_0, \quad (3.23)$$

$$\hat{A} := E\hat{I}, \quad J := 2(E - I)A^{-1}Ba_0 + EL. \quad (3.24)$$

Proof. For brevity, only a sketch of the proof is presented here. In the original control system shown in Fig. 3.2, the gains and biases have discontinuous changes at the switching times $t = kT - \frac{T}{2}$ ($k = 1, 2, 3, \dots$), which makes the signals y and u discontinuous. However, the states and outputs of the plant and compensator (X_c, X_p, v, x) are continuous due to zero feedthrough matrices and the inherent integration actions in the compensator and plant state equations. Hence, the equivalent plant state X_e has discontinuities at the switching times because of g_1 and b_1 (see Eq. (3.8)). Thus, to maintain the equivalence of the simple control system shown in Fig. 3.9 with the original control system over time intervals longer than a half period, we have to intentionally incorporate appropriate jumps in the equivalent plant state X_e at each switching time, which can be described in the following form using Eq. (3.8):

$$\Delta X_{e_k} := X_{e_k}^+ - X_{e_k}^- = \left(\frac{1}{g_{1k}^+} - \frac{1}{g_{1k}^-} \right) X_{p_k} + A_p^{-1}B_p \left(\frac{b_{1k}^+}{g_{1k}^+} - \frac{b_{1k}^-}{g_{1k}^-} \right) \quad (3.25)$$

where the lowest subscript k for each variable refers its value at the switching moment $t = kT - \frac{T}{2}$ ($k = 1, 2, 3, \dots$), and the minus and plus superscripts refer to the values of the corresponding variable at infinitesimal times just before and after the switching moment indicated by the lowest subscript, respectively, as defined in the following forms:

$$X_{p_k} := X_p \left(kT - \frac{T}{2} \right), X_{e_k^+} := X_e \left(kT^+ - \frac{T}{2} \right), X_{e_k^-} := X_e \left(kT^- - \frac{T}{2} \right), \dots \quad (3.26)$$

If we use Eq. (3.8) to replace X_{p_k} by $g_{1_k}^- X_{e_k^-} - F_k^-$ in Eq. (3.25), the equivalent plant state just after the switching moment can be described in terms of its value just before the switching moment as:

$$X_{e_k^+} = \frac{1}{g_{1_k}^+} \left[g_{1_k}^- X_{e_k^-} + A_p^{-1} B_p (b_{1_k}^+ - b_{1_k}^-) \right]. \quad (3.27)$$

The inverse of the plant state matrix is in the following form:

$$A_p^{-1} = \begin{bmatrix} -\varepsilon_1 & -\varepsilon_2 & -\varepsilon_3 & \cdots & -\varepsilon_{n_p-1} & -\varepsilon_{n_p} \\ 1 & 0 & 0 & \cdots & \cdots & 0 \\ 0 & 1 & 0 & \cdots & \cdots & 0 \\ \vdots & \ddots & \ddots & \ddots & \cdots & \vdots \\ 0 & \cdots & 0 & 1 & 0 & 0 \\ 0 & \cdots & \cdots & 0 & 1 & 0 \end{bmatrix} \quad (3.28)$$

Hence, $A_p^{-1} B_p$ is $[-1, 0, \dots, 0]^T$. Using (3.27) and the signal transformation gains and biases selected in (3.1) for the triangular reference, the equivalent plant state at the switching moments can be updated based on the following relationship:

$$X_{e_k^+} = -X_{e_k^-} + L(k - 0.5), \text{ for } k = 1, 2, 3, \dots \quad (3.29)$$

where L is a $n_p \times 1$ vector defined similar to (3.21). Using (3.29) and the fact that the compensator state is continuous at the switching moments, the overall state X just after the switching moment is easily obtained in the form of (3.20). Using the commutativity of multiplication of A^{-1} and e^{At} , the solution of the state X from state-equation (3.16) in the time interval $t \in (kT - \frac{T}{2}, kT + \frac{T}{2})$ with ramp input $r = \frac{2a_0 t}{T}$, in terms of the state just after the switching moment $t = kT - \frac{T}{2}$, can be written in the following form.

$$X(t) = e^{At'} X_k^+ + \{ (e^{At'} - I) [a_0(2k-1)I + A^{-1}\alpha] - \alpha t' I \} A^{-1} B, \quad (3.30)$$

where

$$t' := t - \left(kT - \frac{T}{2} \right), \alpha := \frac{2a_0}{T}, X_k^+ := X(t) \Big|_{t=(kT-\frac{T}{2})^+}. \quad (3.31)$$

Equation (3.19) defines a discrete-time LTI dynamic system with \hat{A} as the state matrix, $[J, H]$ as the input matrix, and $[k - 0.5, 1]^T$ as the input vector whose first element is a discrete-time ramp signal. Hence, a necessary condition for the closed-loop system to be free from exponentially unstable modes is that all eigenvalues of \hat{A} are inside the unit disk. This condition is also a sufficient one because the state at the arbitrary time $t = kT - \frac{T}{2} + t'$ depends on X_k^- through Eqs. (3.20) and (3.30) and variable t' is limited to $t' \in (0, T)$, which shows that if X_k^- does not have any exponentially unstable mode, neither does $X(t)$. In the more general case, where the desired signal x_d is an arbitrary bounded signal but the signal transformation parameters are kept as before with unity DC gain for the plant, Eq. (3.20) will not change but Eqs. (3.30), (3.18), and (3.19) can be represented in the following forms:

$$X(t' + kT - \frac{T}{2}) = e^{At'} X_k^+ + 2(e^{At'} - I)A^{-1}Ba_0k + W(k, t'), \quad (3.32)$$

$$X_1^- = EX_0 + \int_0^{\frac{T}{2}} e^{A(\frac{T}{2}-t)} Bx_d(t) dt, \quad (3.33)$$

$$X_{k+1}^- = \hat{A}X_k^- + Jk + W(k, T) - 0.5EL, \quad k = 1, 2, 3, \dots, \quad (3.34)$$

where

$$W(k, t') = \int_0^{t'} e^{A(t'-\tau)} x_d \left(\tau + kT - \frac{T}{2} \right) d\tau B(-1)^k. \quad (3.35)$$

Since vector $W(k, t')$ is bounded, because of the boundedness of x_d , the aforementioned condition about the absence of exponentially unstable modes is not restricted to the triangular waveform and is also valid for arbitrarily bounded reference inputs.

Theorem 3.3. *Assuming unity DC gain for the plant and signal transformation parameters (3.1), the hybrid control system is free from exponentially unstable modes if and only if the eigenvalues of matrix \hat{A} , defined in (3.24), are inside the unit circle.*

Note that the hybrid control system may have exponentially stable responses, whereas the closed-loop state matrix A , defined in (3.17), may have unstable eigenvalues, which means under some circumstances, incorporation of signal transformation into an ordinary unstable feedback system may stabilize the closed-loop responses.

Steady-State Behavior with Triangular Reference

The signal transformation converts the original triangular reference into a ramp signal. However, it is not desirable for the plant states to grow linearly with time. The following theorem provides conditions under which the states of the plant remain bounded in steady-state conditions.

Theorem 3.4. *Assuming the triangular reference input in Fig. 3.2, unity DC gain for the plant, signal transformation parameters (3.1), and eigenvalues of matrix \hat{A} inside the unit circle, the plant state in the hybrid control system will remain bounded if and only if either of the following conditions is satisfied:*

$$\delta_c := -CA^{-1}B = 1 \quad (3.36)$$

$$P(t') := [I_{n_p}, 0]e^{At'}\hat{I}(I - \hat{A})^{-1}L + 0.5L = 0, \quad \forall t' \in (0, T). \quad (3.37)$$

Proof. Successive use of Eq. (3.19) leads to the following equation:

$$X_{k+1}^- = \hat{A}^k X_1^- + \sum_{l=0}^{k-1} \hat{A}^l [(k-l)J + H - 0.5J], \quad k = 1, 2, 3, \dots, \quad (3.38)$$

which represents the state value just before a generic switching moment in terms of its value just before the first switching moment. We can simplify solution (3.38) if matrix $(I - \hat{A})$ is invertible. Given that eigenvalues of \hat{A} have magnitudes less than 1 this condition is met. Under such assumption, the following equalities hold:

$$\sum_{l=0}^{k-1} (k-l)\hat{A}^l = [\hat{A}^{k+1} - (k+1)\hat{A} + kI](I - \hat{A})^{-2} \quad (3.39)$$

$$\sum_{l=0}^{k-1} \hat{A}^l = (I - \hat{A}^k)(I - \hat{A})^{-1}. \quad (3.40)$$

Substituting the right-hand sides of Eqs. (3.39), (3.40), and (3.18) into Eq. (3.38), we obtain the closed-form formula:

$$X_{k+1}^- = \hat{A}^k EX_1^- + [\hat{A}^{k+1} - (k+1)\hat{A} + kI](I - \hat{A})^{-2}J + (I - \hat{A}^k)(I - \hat{A})^{-1}(H - 0.5J), \quad (3.41)$$

which is valid for $k = 1, 2, 3, \dots$, and represents the overall state just before the switching moment $t = kT + \frac{T}{2}$ in terms of the state just before the first switching moment initial state. For a stable closed-loop system, where the eigenvalues of matrix \hat{A} are within the unit circle, $\lim_{k \rightarrow \infty} \hat{A}^k$ is zero and (3.41) is reduced to the following relationship:

$$\lim_{k \rightarrow \infty} X_{k+1}^- = (I - \hat{A})^{-1}[J(k+0.5) + H - (I - \hat{A})^{-1}J] \quad (3.42)$$

Using (3.42) with k replaced by $k-1$, (3.20), and (3.30), the steady-state expression for $X(t)$ is obtained as

$$\lim_{k \rightarrow \infty} X \left(kT - \frac{T}{2} + t' \right) = Q(t')k + U(t'), \quad t' \in (0, T), \quad (3.43)$$

where

$$Q(t') = e^{A't'} [\hat{I}(I - \hat{A})^{-1}J + L + 2A^{-1}Ba_0] - 2A^{-1}Ba_0 \quad (3.44)$$

$$U(t') = e^{A't'} [\hat{I}(I - \hat{A})^{-1}(H - 0.5J) - \hat{I}(I - \hat{A})^{-2}J - 0.5L] \\ + [(e^{A't'} - I)(A^{-1} - \frac{T}{2}I) - t'I]A^{-1}B\alpha. \quad (3.45)$$

Since the DC gain of the equivalent plant in Fig. 3.9 is unity, and the DC gain from input v to state vector X_e is $-A_p^{-1}B_p = [1, 0, \dots, 0]^T$, the DC gain of the closed-loop system from input r to the overall state X , considering no signal transformation, is

$$-A^{-1}B = \begin{bmatrix} -A_p^{-1}B_p\delta_c \\ V \end{bmatrix} = \begin{bmatrix} \delta_c \\ 0_{(n_p-1) \times 1} \\ V \end{bmatrix}, \quad (3.46)$$

where vector V describes the closed-loop DC gain from r to the compensator state X_c , and δ_c is the closed-loop DC gain from input r to output y . Using (3.24), (3.22), (3.46), and the fact that $\hat{I}^{-1} = \hat{I}$, the coefficient of k in (3.43) can be simplified to

$$Q(t') = e^{A't'} \hat{I}(I - \hat{A})^{-1}L(\delta_c - 1) - 2A^{-1}Ba_0. \quad (3.47)$$

Using (3.8), (3.1), (3.15), and (3.43), one can show that the plant state in steady-state can be described as

$$\lim_{k \rightarrow \infty} X_p \left(kT - \frac{T}{2} + t' \right) = g_1 \{ [I_{n_p}, 0]Q(t') + 2A_p^{-1}B_p a_0 \} k + g_1 [I_{n_p}, 0]U(t'). \quad (3.48)$$

Using equality $-A_p^{-1}B_p = [1, 0, \dots, 0]^T$, (3.47), and (3.46) in (3.48), the coefficient of k in the steady-state solution of the plant state vector can be expressed in the following form:

$$(-1)^k P(t')(\delta_c - 1), \quad (3.49)$$

which reveals that the plant state tends to a bounded value if and only if either the closed-loop DC gain δ_c is unity, or all the elements in the time-dependent vector $P(t')$, defined in (3.37), are identically zero.

Since condition (3.37) is almost impossible to occur, condition (3.36) is almost a necessary condition for boundedness of the plant state. The plant does not have any pole at the origin because of its unity DC gain. Hence, the only way for the closed-loop system to have a unity DC gain is that the compensator has at least one pole at the origin. Thus, a *sufficient and almost necessary* condition for boundedness of the plant state is that the compensator has at least one pole at the origin.

In the more general case of an arbitrary bounded reference signal x_d , using (3.34), the constant vector $H - 0.5J$ in (3.38) should be replaced by the bounded vector $W(k-l, T) - 0.5EL$. In this case, the last term in the right-hand side of (3.41) should be replaced by $\sum_{l=0}^{k-1} \hat{A}^l [W(k-l, T) - 0.5EL]$, which will not grow with k , because the state matrix \hat{A} in the discrete-time LTI system (3.34) is stable. In this way, all of

the terms in the right-hand sides of Eqs. (3.42), (3.43), and (3.48), which grow with k , remain unchanged. Hence, the aforementioned condition about the boundedness of the plant state is not restricted to the triangular desired waveform and is valid for any arbitrary bounded reference signal x_d as well.

Theorem 3.5. *Assuming unity DC gain for the plant, signal transformation parameters (3.1), and eigenvalues of matrix \hat{A} within the unit circle, a sufficient and almost necessary condition for the plant state to remain bounded in the hybrid control system is that the compensator has at least one pole at the origin.*